Microphase Separation of ABC-Type Triblock Copolymers

Hatsumi Nakazawa and Takao Ohta*

Department of Physics, Ochanomizu University, Tokyo 112, Japan

Received April 27, 1993; Revised Manuscript Received July 13, 1993•

ABSTRACT: We have studied microphase separation of ABC-type triblock copolymers in the strong segregation limit by generalizing our previous theory for diblock copolymers. The free energy functional in terms of local monomer concentrations is derived via a mean field approximation and a local approximation for higher order coupling. In the special case where the monomer number of the A block is the same as that of the C block, we calculate the critical values of the volume fraction for morphological transitions of ordered domains from lamellar to cylinder and from cylinder to sphere. It is emphasized that in the ABC-tpye copolymer, a square lattice is predicted to be more stable than a hexagonal one for cylindrical domains. The possibility of an ordered tricontinuous diamond structure is also examined. The results are compared with the recent experiments by Matsushita et al.

1. Introduction

Recently, statistical mechanical theory has been developed to understand ordered phases in microphase-separated block copolymer melts. In particular, there are several theories for diblock copolymers. Helfand and coworkers[1] have studied the equilibrium state of AB-type block copolymers in the strong segregation limit. In order to obtain the microphase-separated phase, they employ an analogy of a Brownian particle moving in a potential caused by the concentration variation, which is determined self-consistently. Semenov[2] has also studied the strong segregation case by an electrostatic analogy. On the other hand, Leibler[3] has considered the weak segregation case by means of a density expansion method. Ohta and Kawasaki[4,5] have emphasized the relevancy of the long range interaction of the concentration fluctuations in the strong segregation limit. The long range interaction is originated from the restriction of polymer chain conformation because of the chain connectivity. The critical block ratios of morphological changes obtained in ref 4 are more in accord with experiments compared to other theories. Quite recently, further development of the theory has been carried out, which covers both weak and strong segregation limits. One is a numerical study based on a model similar to that in ref 4 to obtain the phase diagram.[6] On the other hand, Shull[7] has employed a discretized version of the theory of ref 1 and calculated numerically the equilibrium repeat period of a lamellar structure. See also ref 8. Thus the theory of diblock copolymers has now been developed quite intensively.

Matsushita et al.[9,10] have experimentally studied microphase separation of ABC-type triblock copolymers composed of poly(isoprene-*b*-styrene-*b*-2-vinylpyridine). They synthesized a series of samples so that the volume fraction of the middle block polymer, polystyrene, ranges from 0.3 to 0.8; while the volume fractions of the two end segments are equal. By transmission electron microscopy and X-ray scattering technique, they have observed several types of ordered structures. Besides the usual lamellar phase for fairly small volume fractions of the middle polymer, a tetragonal structure of cylindrical domains, a tricontinuous diamond structure and bcc structure of spherical domains are identified by changing the volume fraction.

In these experiments, there are several findings which are characteristic features of ABC-type triblock copolymers. First of all, cylindrical domains constitute a square lattice. This is different from the diblock case where a hexagonal lattice has been observed[11] and it is confirmed theoretically.[1,2,4] However the reason as to why a tetragonal structure in ABC copolymers is more favorable can be understood intuitively. Cylindrical domains of A and C segments with equal length cannot constitute identical sublattices with 6-fold symmetry. The situation is analogous to an antiferromagentic Ising model with a short range interaction on a hexagonal lattice where frustration of spin configuration occurs in the ordered phase. In the present problem, an A (C) domain corresponds to the spin up (down) state.

Another interesting ordered phase is an ordered tricontinuous diamond structure. Although a diamond structure has been reported for AB star block[12,13] and diblock[14] copolymers and blends of AB diblock copolymer and a parent homopolymer,[15] experiments by Matsushita et al.[10] show that the diamond structure appears in a wider regime of the volume fraction compared to the case of diblock copolymers.

In this paper, we generalize our theory of ref 4 to ABC-type triblock copolymers to study the morphological transitions and to compare predicted phase behavior with recent experimental results. The free energy functional for the local concentrations is derived in terms of the local monomer densities. The equilibrium free energy is calculated by means of a variational method for each ordered structure in the strong segregation limit. The theory employs two main approximations. One is a mean field approximation in the derivation of the free energy functional. This is justified since the system we consider is a concentrated copolymer. The other approximation neglects nonlocality in the higher order coupling for the density expansion of the free energy functional. Unfortunately, the significance of higher order corrections is quite difficult to estimate. We have not obtained any definite conclusion for the nonlocal effects in the higher order coupling of the diblock case.[17] (It is noted here that what we ignore is not higher order coupling itself but the nonlocality that appears there.) Shull[7] has shown in his generalized theory of ref 1, which is free from the above approximation, that the ratio of the equilibrium period in the strong segregation limit to the radius of gyration in the disordered state is as large as about 15% compared to that obtained by the truncation approximation.[6]

* To whom any correspondence should be addressed.

• Abstract published in *Advance ACS Abstracts*, September 1, 1993.

0024-9297/93/2226-5503$04.00/0 © 1993 American Chemical Society

In a recent paper, Spontak and Zielinski[16] have studied the microphase separation of ABC-type triblock copolymers by using a confined single-chain model. However, morphological transitions were not considered since they were concerned only with the lamellar structure as were other more refined theories for the diblock case.[7,8] As was mentioned above, application of our theory[4] to diblock copolymers has predicted critical volume fractions of morphological transition in good agreement with experiments. The present study of triblock copolymers will provide another check of the theory.

Organization of the paper is as follows. In section 2, the free energy functional of ABC-type triblock copolymers is derived. The equilibrium free energy of lamellar, cylindrical, and spherical structures is calculated in section 3. We consider the diamond structure separately in section 4. The final section (section 5) is devoted to discussions. Some details in the derivation of the free energy functional are described in Appendix A, while the form factor of a tetrapod used in section 4 is calculated approximately in Appendix B.

2. Model and Free Energy Functional

In this section, we derive the free energy of triblock copolymers in terms of the monomer concentrations. We consider a monodisperse system having n polymer chains with chain length N. Each chain consists of three different monomers, A, B, and C, where the B segment is in the middle of the chain. The length of the A and C segments is denoted by Nf_A and Nf_C, respectively. We start with the model Hamiltonian for flexible chains with a short range interaction:

$$H\{\mathbf{r}_i(\tau)\} = H_0\{\mathbf{r}_i(\tau)\} + H_1\{\mathbf{r}_i(\tau)\} \tag{2.1}$$

where

$$H_0\{\mathbf{r}_i(\tau)\} = \frac{1}{2}\sum_{i=1}^{n}\int_0^N d\tau\left(\frac{d\mathbf{r}_i(\tau)}{d\tau}\right)^2 \tag{2.2}$$

$$H_1\{\mathbf{r}_i(\tau)\} = \frac{1}{2}\sum_{\alpha,\beta} w_{\alpha\beta}\sum_{i,j}\int_\alpha d\tau\int_\beta d\tau'\,\delta(\mathbf{r}_i(\tau) - \mathbf{r}_j(\tau')) \tag{2.3}$$

The position of the monomer at the contour length τ of the ith chain is denoted by $\mathbf{r}_i(\tau)$. The constant $w_{\alpha\beta}$ (α, β = A, B, and C) denotes the interaction strength. The suffix in each integral symbol in eq 2.3 indicates the region of the integral such that $0 < \tau < Nf_A$ for A, $Nf_A < \tau < N(1 - f_C)$ for B, and $N(1 - f_C) < \tau < N$ for C. Let us introduce the monomer densities:

$$\hat{\rho}_\alpha(\mathbf{r}) = \sum_{i=1}^{n}\int_\alpha d\tau\,\delta(\mathbf{r} - \mathbf{r}_i(\tau)) \tag{2.4}$$

Our aim in this section is to write the partition function Z as

$$Z = \int d\{\mathbf{r}_i\}\exp[-H\{\mathbf{r}_i(\tau)\}] = \int d\{\rho_\alpha\}\exp[-F\{\rho_\alpha\}] \tag{2.5}$$

We have used the unit $k_BT = 1$ where k_B is the Boltzmann constant and T temperature. The method of deriving $F\{\rho_\alpha\}$ is essentially the same as that for diblock copolymers.[4] We describe only the outline here. The first step is to use the identity

$$\int d\{\rho_\alpha\}\prod_{\mathbf{r}}\delta(\rho_\alpha(\mathbf{r}) - \hat{\rho}_\alpha(\mathbf{r})) = 1 \tag{2.6}$$

so that the partition function can be written as

$$Z = \int d\{\rho_\alpha\}\int d\{\phi_\alpha\}\exp[-G\{\phi_\alpha\} + i\int d\mathbf{r}\sum_\alpha \phi_\alpha\rho_\alpha] \tag{2.7}$$

where

$$G\{\phi_\alpha\} = H_1\{\rho_\alpha\} - \ln\int d\{\mathbf{r}_i\}\exp[-i\int d\mathbf{r}\sum_\alpha \phi_\alpha(\mathbf{r})\hat{\rho}_\alpha(\mathbf{r}) - H_0\{\mathbf{r}_i(\tau)\}] \tag{2.8}$$

with

$$H_1\{\rho_\alpha\} = \frac{1}{2}\sum_{\alpha\beta}\int d\mathbf{r}\, w_{\alpha\beta}\rho_\alpha(\mathbf{r})\rho_\beta(\mathbf{r}) \tag{2.9}$$

Equation 2.8 can be evaluated by the expansion in powers of ϕ_α. Apart from an additive constant, G is obtained as

$$G\{\phi_\alpha\} = \sum_{\alpha\beta}\int d\mathbf{r}\int d\mathbf{r}'\left[\frac{1}{2}\Gamma_{\alpha\beta}(\mathbf{r},\mathbf{r}')\phi_\alpha(\mathbf{r})\phi_\beta(\mathbf{r}')\right] + W'\{\phi_\alpha\} \tag{2.10}$$

where $W'\{\phi_\alpha\}$ contains the higher order terms together with the interaction part $H_1\{\rho_\alpha\}$ and $\Gamma_{\alpha\beta}(\mathbf{r},\mathbf{r}')$ is the density correlation function of a single Gaussian chain:

$$\Gamma_{\alpha\beta}(\mathbf{r},\mathbf{r}') = \langle\hat{\rho}_\alpha(\mathbf{r})\hat{\rho}_\beta(\mathbf{r}')\rangle_0 - \langle\hat{\rho}_\alpha(\mathbf{r})\rangle_0\langle\hat{\rho}_\beta(\mathbf{r}')\rangle_0 \tag{2.11}$$

The bracket $\langle\ldots\rangle_0$ indicates the average with respect to H_0.

It should be noted that the average value $\langle\hat{\rho}_\alpha(\mathbf{r})\rangle_0$ has been subtracted in the correlation (2.11) in order to eliminate a term linear in ϕ_α in (2.10). Accordingly, hereafter we replace the monomer density ρ_α by $\rho_\alpha - \bar{\rho}_\alpha$ where $\bar{\rho}_\alpha$ is the spatial average of ρ_α.

The next step is to carry out the integral over ϕ_α in (2.7). However an exact evaluation is impossible. Here we employ a mean field approximation. This is, we replace ϕ_α by its extremum ϕ_α^* defined through the relation

$$\frac{\delta G}{\delta\phi_\alpha^*} = i\rho_\alpha(\mathbf{r}) \tag{2.12}$$

and put

$$F\{\rho_\alpha\} = G\{\phi_\alpha^*\} - i\sum_\alpha\int d\mathbf{r}\,\phi_\alpha^*\rho_\alpha \tag{2.13}$$

Since this is a Legendre transformation, we have another relation

$$\frac{\delta F}{\delta\rho_\alpha} = -i\phi_\alpha^* \tag{2.14}$$

We solve (2.12) to express ϕ_α^* in terms of ρ_α. Substituting the result into (2.14), we can obtain $F\{\rho_\alpha\}$ term by term. The final form is given by

$$F\{\rho_\alpha\} = \sum_{\alpha\beta}\int d\mathbf{r}\left[\frac{1}{2}\mathrm{M}^{\alpha\beta}(\mathbf{r},\mathbf{r}')\rho_\alpha(\mathbf{r})\rho_\beta(\mathbf{r}')\right] + W\{\rho_\alpha\} \tag{2.15}$$

where W comes from W' in (2.9) and $\mathrm{M}^{\alpha\beta}(\mathbf{r},\mathbf{r}')$ is the inverse matrix of Γ defined through the relation

$$\sum_\gamma\int d\mathbf{r}''\,\mathrm{M}^{\alpha\gamma}(\mathbf{r},\mathbf{r}'')\Gamma_{\gamma\beta}(\mathbf{r}'',\mathbf{r}') = \delta_{\alpha\beta}\delta(\mathbf{r} - \mathbf{r}') \tag{2.16}$$

Using the formula (2.11), the matrix M can be calculated exactly. Some of the properties of M are summarized in Appendix A.

In a real copolymer melt, we may impose the incompressibility condition:

$$\rho_A(\mathbf{r}) + \rho_B(\mathbf{r}) + \rho_C(\mathbf{r}) = 0 \tag{2.17}$$

Recall that $\rho_\alpha(\mathbf{r})$ is a deviation around its spatial average. We eliminate $\rho_B(\mathbf{r})$ in the free energy (2.15) so that it becomes

$$F\{\rho_\alpha\} = \frac{1}{2}\sum_{\alpha\beta}\int_{\mathbf{q}} M_{\mathbf{q}}^{\alpha\beta}\rho\alpha_{\mathbf{q}}\rho_{\beta-\mathbf{q}} + W\{\rho_\alpha\} \tag{2.18}$$

where $\int_{\mathbf{q}} = \int d\mathbf{q}/(2\pi)^d$ with d the dimensionality of space. The Fourier component $\rho_{\mathbf{q}}$ has been defined by

$$\rho_{\mathbf{q}} = \int d\mathbf{r}\rho(\mathbf{r}) \exp(i\mathbf{q}\cdot\mathbf{r}) \tag{2.19}$$

The matrix M is now a 2×2 matrix. As in the previous study,[4] we employ an interpolation formula for M since the q dependence is complicated. Let us put each component of M as

$$M_{\mathbf{q}}^{\alpha\beta} + A_S^{\alpha\beta}\frac{1}{n^2N}q^2 + A_L^{\alpha\beta}\frac{1}{n^2N^3}\frac{1}{q^2} \tag{2.20}$$

where $A_S^{\alpha\beta}$ and $A_L^{\alpha\beta}$ are obtained from $M_{\mathbf{q}}^{\alpha\beta}$ in the limits $q \to \infty$ and $q \to 0$, respectively. Using the results in Appendix A we have

$$A_S^{AA} = A\frac{1-f_C}{f_A} \qquad A_S^{AC} = A_S^{CA} = A \qquad A_S^{CC} = A\frac{1-f_A}{f_C} \tag{2.21}$$

where

$$A = \frac{1}{4(1-f_A-f_C)} \tag{2.22}$$

and

$$A_L^{AA} = B\frac{2(1-f_C)^2}{f_A^2} \qquad A_L^{AC} = A_L^{CA} = B\frac{1-f_A^2-f_C^2}{f_Af_C}$$

$$A_L^{CC} = B\frac{2(1-f_A)^2}{f_C^2} \tag{2.23}$$

where

$$B = \frac{6}{\{3-2(f_A+f_C)-(f_A-f_C)^2\}(1-f_A-f_C)^2} \tag{2.24}$$

Substituting (2.20) into (2.18) yields the free energy written as

$$F\{\rho_\alpha\} = F_L\{\rho_\alpha\} + F_S\{\rho_\alpha\} \tag{2.25}$$

where

$$F_L\{\rho_\alpha\} = \frac{1}{n^2N^3}\frac{1}{2}\sum_{\alpha\beta}\int_{\mathbf{q}} A_L^{\alpha\beta}\frac{1}{q^2}\rho_{\alpha\mathbf{q}}\rho_{\beta-\mathbf{q}} \tag{2.26}$$

$$F_S\{\rho_\alpha\} = \frac{1}{n^2N}\frac{1}{2}\sum_{\alpha\beta}\int_{\mathbf{q}} A_S^{\alpha\beta}q^2\rho_{\alpha\mathbf{q}}\rho_{\beta-\mathbf{q}} + W\{\rho_\alpha\} \tag{2.27}$$

In (2.26), the $q = 0$ component should be excluded from the summation.

A remark is now in order. The long range part (2.26) does not reduce to that of an AC diblock copolymer[4] in the limit $f_B \to 0$. This is because the middle segment ρ_B with a finite length has been eliminated to obtain (2.26). If we take the limit $f_B \to 0$ in (2.15), it indeed agrees with the AC diblock free energy functional.

Hereafter we ignore the nonlocality in $W\{\rho_\alpha\}$. That is, we employ the local approximation for the higher order coupling in ρ. We assume that $W\{\rho_\alpha\}$ has four degenerate deep local minima in the $\rho_A - \rho_C$ plane so that the system is in a strongly segregated microphase-separated state. The local approximation is most crude. We do not have any justification of it at present although the theory[4] has successfully predicted the morphological transitions in diblock copolymers.

3. Lamellar, Cylindrical, and Spherical Domains

3-1. Free Energy for Spatially Periodic Structures. Now we calculate the free energy for the microphase-separated states in the strong segregation limit. In the present system we have to consider two kinds of domains, A and C domains. Corresponding to the experimental conditions,[9,10] hereafter we assume $f_A = f_C \equiv f$. Therefore a periodic structure consists of two identical sublattices in the matrix of B domains, which we call A and C sublattices. We denote the center of gravity of a domain in the A sublattice by $\mathbf{r} = n_1\mathbf{a} + n_2\mathbf{b} + n_3\mathbf{c}$ where n_i (i = 1–3) are any integers and **a**, **b**, and **c** are the primitive translation vectors. Suppose that the C sublattice can be constructed by uniform translation of the A sublattice by the vector **e**. The long range part of the free energy can be written as

$$F_L = \frac{L^3}{2n^2N^3}\sum_{\alpha\beta}\sum_{\mathbf{Q}}\frac{1}{\mathbf{Q}^2}A_L^{\alpha\beta}\Psi_\alpha(\mathbf{Q})\Psi_\beta^*(\mathbf{Q}) \tag{3.1}$$

where **Q** is the reciprocal lattice vector of the sublattice. $\Psi_\alpha(\mathbf{Q})$ is the form factor of an α domain, and L is the linear dimension of the system. By using the translation vector **e**, $\Psi_C(\mathbf{Q})$ is written as

$$\Psi_C(\mathbf{Q}) = \Psi_A(\mathbf{Q}) \exp(i\mathbf{Q}\cdot\mathbf{e}) \tag{3.2}$$

In the strong segregation limit, the short range part of the free energy is simply given by the interfacial energy times the total interfacial area:

$$F_S = \frac{2}{n^2N}S_AM_A\sigma_A \tag{3.3}$$

where S_α is the interfacial area of an α domain and M_α is the total number of α domains. The interfacial energy σ_α is defined here by

$$\sigma_\alpha = A_S^{\alpha\alpha}\int d\mathbf{r}\left(\frac{d\Psi_\alpha}{d\mathbf{r}}\right)^2 \tag{3.4}$$

Note that σ_α in (3.4) is independent of the chain length N. It should also be independent of the block ratio in the strong segregation limit.[5] Here we are not interested in the actual value of σ_α since it is factorized out in the equilibrium free energy (3.11) and (3.12) below so that the critical block ratio for the morphological transitions is not affected by the value of the interfacial tension. In (3.3) we have used the assumption that $f_A = f_C$ and the equivalence of microscopic properties of the A and C monomers, such as the Kuhn statistical length, i.e., $M_A = M_C$, $S_A = S_C$, and $\sigma_A = \sigma_C$. In the following, we calculate the free energy of the ordered structures by using (3.1) and (3.3).

3-2. Lamellar Domains. In a lamellar structure, domains are supposed to array periodically in the x-direction with sequence such as ABCBA. We denote the period by l. The width of the A and C domains are equal

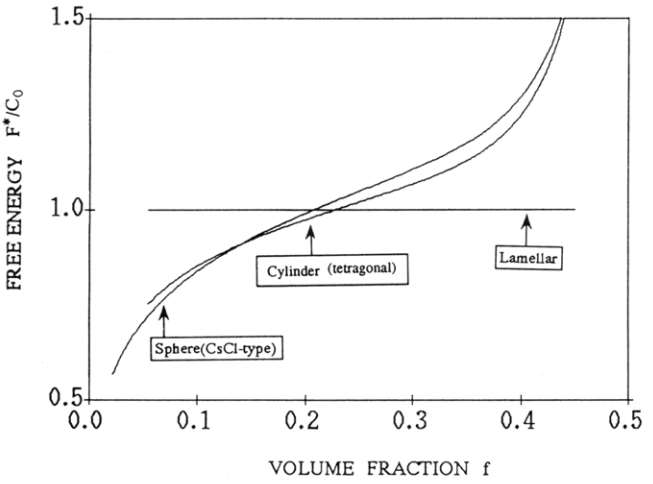

Figure 1. Equilibrium free energy F^*/C_0 for lamellar, cylindrical, and spherical structures.

to fl. The form factor of an A domain is given by

$$\Psi_A(\mathbf{Q}) = \frac{1}{l}\frac{1}{iQ}\{\exp(ifl\mathbf{Q}) - 1\} \tag{3.5}$$

Since $\mathbf{e} = (l/2)\mathbf{e}_x$ with $\mathbf{e}_x$ the unit vector in the x direction and $Q = 2\pi m/l$ with m integers, we have

$$\mathbf{Q}\cdot\mathbf{e} = \pi m \tag{3.6}$$

Substituting (3.5) and (3.6) into (3.1) yields

$$F_L = \frac{1}{2\rho_0 nN}\left(\frac{l^2\Phi}{N}\right) \tag{3.7}$$

where $\rho_0 = nN/L^3$ and

$$\Phi = \sum_{\hat{\mathbf{Q}}}\frac{1}{\hat{Q}^2}\{2A_L^{AA} + 2A_L^{AC}\exp(i\mathbf{Q}\cdot\mathbf{e})\}\Psi_A(\hat{\mathbf{Q}})\Psi_A^*(\hat{\mathbf{Q}}) \tag{3.8}$$

with $\hat{\mathbf{Q}} = \mathbf{Q}l$. Note that Φ is a function only of f. Since $M_A = L/l$, the short range part F_S, is, on the other hand, given by

$$F_S = \frac{1}{\rho_0 nN}\left(\frac{2N\sigma_A\hat{\gamma}}{l}\right) \tag{3.9}$$

with $\hat{\gamma} = 2$. This factor arises from the fact that there are two interfaces per domain. Minimization of $F = F_L + F_S$ with respect to l gives us the equilibrium period l^* and the equilibrium free energy F^*

$$l^* = \left(\frac{2\sigma_A\hat{\gamma}N^2}{\Phi}\right)^{1/3} \tag{3.10}$$

$$F^* = C_0(\hat{\gamma}^2\Phi)^{1/3} \tag{3.11}$$

where

$$C_0 = \frac{3}{\rho_0 nN}\left(\frac{N\sigma_A{}^2}{2}\right)^{1/3} \tag{3.12}$$

The result (3.10) means the two-thirds power law dependence of the equilibrium period. The same result has been obtained for a diblock case[4] and has been confirmed experimentally. In Figure 1, the free energy F^* is plotted as a function of f.

3-3. Cylindrical Domains. Next we consider a cylindrical morphology of A and C domains which is expected to appear for smaller values of f. In the case of

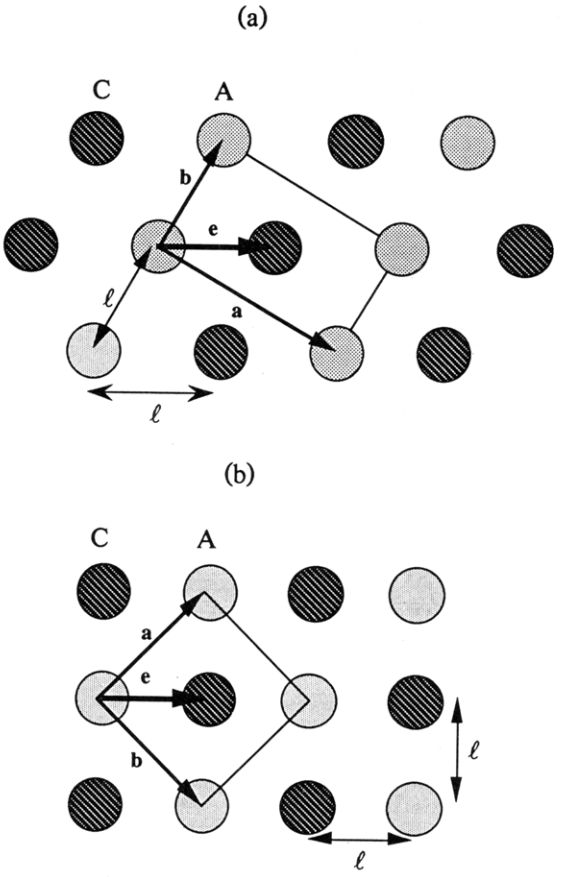

Figure 2. (a) Hexagonal structure of cylindrical A and C domains. (b) Tetragonal structure of cylindrical A and C domains.

diblock copolymers, a hexagonal lattice is most favorable, as is observed experimentally.[11] However, the situation is quite different for a triblock case, especially when the A and C segments have the same block length. If they constitute a hexagonal lattice, the sublattice should be a rectangular structure and, hence, each chain has to distort anisotropically in space.

Here we examine two structures. One is a hexagonal lattice, and the other is a square lattice. First let us consider a hexagonal lattice of disk-shaped domains with the radius R and with the lattice constant l. The primitive translation vectors $\mathbf{a}$ and $\mathbf{b}$ are defined as shown in Figure 2a. Then the reciprocal lattice vectors are given by

$$\mathbf{Q} = m_1\mathbf{A} + m_2\mathbf{B} \tag{3.13}$$

with m_1 and m_2 integers and $\mathbf{A} = 2\pi\mathbf{a}/3l^2$ and $\mathbf{B} = 2\pi\mathbf{b}/l^2$. The vector $\mathbf{e}$ which connects the two sublattices is given by $\mathbf{e} = (\sqrt{3}l/2, l/2)$. Hence we have

$$\mathbf{Q}\cdot\mathbf{e} = \pi(m_1 + m_2) \tag{3.14}$$

The form factor of an A domain is given by

$$\Psi_A(\mathbf{Q}) = \frac{1}{v_A}\int d\mathbf{r}\,\Psi_A(\mathbf{r})\exp(i\mathbf{Q}\cdot\mathbf{r})$$
$$= \frac{2f}{\hat{Q}}J_1(\hat{\mathbf{Q}}) \tag{3.15}$$

where $v_A = \sqrt{3}l^2L$, $\hat{\mathbf{Q}} = \mathbf{Q}R$, and $J_1(x)$ is the Bessel function of first kind. In (3.15) we have used the relation $f = \pi R^2/\sqrt{3}l^2$.

The long range part of the free energy is the same as (3.7) if we replace l by R there. The f-dependent part Φ is also the same form as (3.8) but with (3.13), (3.14), and

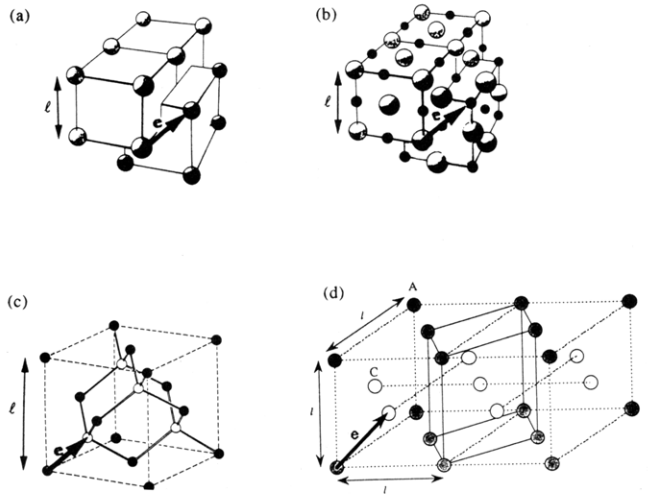

Figure 3. (a) CsCl-type structure of spherical domains. (b) NaCl-type structure. (c) Wurtzite structure. The bond connected A (black) and C (white) domains have no meaning. (d) fcc structure of A (white) and C (black) domains.

(3.15). The short range part is given by

$$F_S = \frac{1}{\rho_0 nN}\left(\frac{2N\sigma_A\hat{\gamma}}{R}\right) \tag{3.16}$$

where $\hat{\gamma} = 2f$.

The structure with a tetragonal symmetry can be treated similarly. The reciprocal lattice vectors $\mathbf{Q}$ are given by (3.13) with $\mathbf{A} = \pi\mathbf{a}/l^2$ and $\mathbf{B} = \pi\mathbf{b}/l^2$, where $\mathbf{a}$ and $\mathbf{b}$ are defined as in Figure 2b. The ratio R/l is given by $R/l = (2f/\pi)^{1/2}$. Other formulas (3.14) and (3.15) are unchanged to calculate F_L. The short range part is given by (3.16) irrespective of the lattice symmetry.

The lattice sum contained in Φ was evaluated numerically. It is found that the free energy for a square lattice is lower than that of a hexagonal lattice for $f < 0.36$. Furthermore it becomes smaller than that of a lamellar structure at $f = 0.23$, as shown in Figure 1. Thus we conclude that the critical block ratio f_{lc} between the lamellar and the cylindrical morphology is $f_{lc} = 0.23$ and that cylindrical domains constitute a square lattice.

We have examined more general structures by changing the angle ϕ between the vectors $\mathbf{b}$ and $\mathbf{e}$ in Figure 2a. That is, we have calculated the free energy for $\pi/3 < \phi < \pi/2$ for each f. The minimum of the free energy always occurs at $\phi = \pi/2$ for $f < 0.28$. Thus the square lattice is indeed the most stable one.

3-4. Spherical Domains. If one decreases the block ratio f further, dispersed micelles of A and C domains appear, which constitute a three-dimensional lattice. We have examined various possible structures, as shown in Figure 3. Parts a and b of Figure 3 were taken from ref 18, while Figure 3c was taken from ref 19. Since the calculation of the free energy is essentially the same for these structures, we shall describe below only the case of a CsCl-type bcc structure in some detail.

The form factor of a sphere with radius R is given by

$$\Psi_A(\mathbf{Q}) = \frac{1}{v_A}\int d\mathbf{r}\, \Psi_A(\mathbf{r}) \exp(i\mathbf{Q}\cdot\mathbf{r})$$

$$= \frac{3f}{\hat{Q}^3}\{\sin\hat{Q} - \hat{Q}\cos\hat{Q}\} \tag{3.17}$$

where $v_A = 4\pi R^3/3f$ and $\hat{Q} = QR$. The translation vector

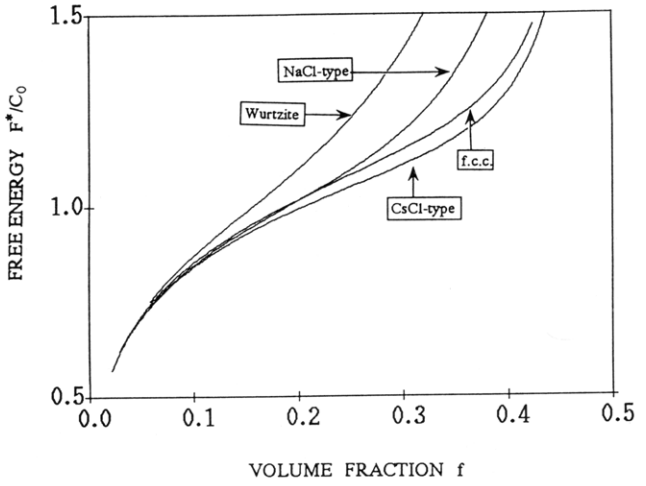

Figure 4. Equilibrium free energy for various three-dimensional structures.

$\mathbf{e}$ between the two sublattices is given by

$$\mathbf{e} = \left(\frac{l}{2}, \frac{l}{2}, \frac{l}{2}\right) \tag{3.18}$$

where l is defined in Figure 3a and related to R as $R/l = (3f/4\pi)^{1/3}$. The reciprocal lattice vectors $\mathbf{Q}$ are given by

$$\mathbf{Q} = \left(\frac{2\pi}{l}m_1, \frac{2\pi}{l}m_2, \frac{2\pi}{l}m_3\right) \tag{3.19}$$

with m_i integers. Thus we have

$$\mathbf{Q}\cdot\mathbf{e} = \pi(m_1 + m_2 + m_3) \tag{3.20}$$

The long range part takes the form of

$$F_L = \frac{1}{2\rho_0 nN}\left(\frac{R^2\Phi}{N}\right) \tag{3.21}$$

where Φ is given by (3.8) together with (3.17)–(3.20). The short range part becomes as

$$F_S = \frac{1}{\rho_0 nN}\left(\frac{2N\sigma_A\hat{\gamma}}{R}\right) \tag{3.22}$$

with $\hat{\gamma} = 3f$. Equation 3.22 is independent of the lattice structure.

The results of numerical calculation are displayed in Figure 4. It is found that the CsCl-type structure yields the lowest equilibrium free energy for the whole range of f. This free energy is also shown in Figure 1 in comparison with lamellar and cylindrical cases. We note that the microdomain structural transition from cylinder to sphere occurs at $f \equiv f_{cs} = 0.14$.

4. Diamond Structure

Besides the ordered structures considered in the previous section, a more complicated structure called a diamond structure has been observed experimentally in AB diblock[14] and star block[12,13] copolymers, in blends[15] of a diblock copolymer and a homopolymer, and in ABC triblock copolymers.[9,10] Matsushita et al. have found that a double diamond structure appears over the range $0.17 < f < 0.26$ in their symmetric ABC triblock copolymers.[10]

A skeleton of the A domains in the diamond structure is shown in Figure 5a. The unit cell of the diamond structure consists of two sublattices of fcc structure, which are translated with each other by the vector $\boldsymbol{e} = (a/4, a/4, a/4)$ with a the size of the unit cell as shown in the figure. Note that this vector $\boldsymbol{e}$ is different from the translation vector introduced in the previous section. (Actually, the

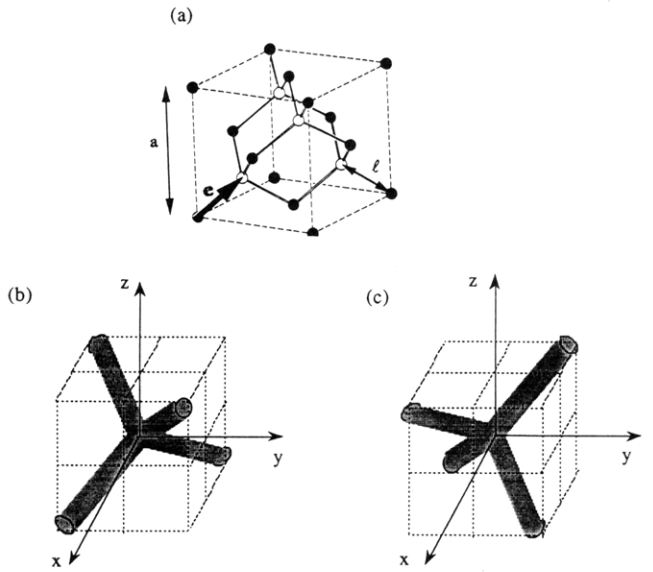

Figure 5. (a) Skeleton of A domains in the diamond structure. (b) Tetrapod whose center is on the black dots in Figure 5a. (c) Tetrapod whose center is on the white dots in Figure 5a.

diamond structure of C domains which is not shown in Figure 5a is given by displacing A domains by the factor $2\boldsymbol{e}$). Two kinds of tetrapods shown in Figures 5b,c are placed on each sublattice so that a continuous diamond structure is constructed. The nearest neighbor distance of the lattice points in the diamond structure is denoted by l which is related to the cell size a as $l = \sqrt{3}a/4$.

Now we express the long range part of the free energy in terms of the form factor of a tetrapod shown in Figure 5b, which is denoted by $\Psi_T(\mathbf{Q})$. The form factor of the other tetrapod shown in Figure 5c is simply given by its complex conjugate $\Psi_T^*(\mathbf{Q})$. The Fourier transform of $\rho_A(\mathbf{r})$ is, then, given by

$$\Psi_A(\mathbf{Q}) = \frac{1}{2v_T}\int d\mathbf{r}\, \rho_A(\mathbf{r}) \exp(i\mathbf{Q}\cdot\mathbf{r}) + \frac{1}{2v_T}\int d\mathbf{r}\, \rho_A(\mathbf{r}) \exp(-i\mathbf{Q}\cdot\mathbf{r} + i\mathbf{Q}\cdot\boldsymbol{e})$$
$$= \Psi_T(\mathbf{Q}) + \Psi_T^*(\mathbf{Q}) \exp(i\mathbf{Q}\cdot\boldsymbol{e}) \quad (4.1)$$

where $v_T = (8/3\sqrt{3})l^3$ and $\mathbf{Q}$ is the reciprocal lattice vector of the fcc sublattice: $Q_x = (2\pi/a)(m_1 - m_2 + m_3)$, $Q_y = (2\pi/a)(m_1 + m_2 - m_3)$, and $Q_z = (2\pi/a)(-m_1 + m_2 + m_3)$ with m_i (i = 1–3) integers. The integrals in the first and the second terms run inside the cube shown in Figures 5b,c, respectively. The factor $^1/_2$ appears in (4.1) since there are two kinds of tetrapod. The Fourier transform of $\rho_C(\mathbf{r})$ is given by

$$\Psi_C(\mathbf{Q}) = \Psi_A(\mathbf{Q}) \exp(2i\mathbf{Q}\cdot\boldsymbol{e}) = \Psi_T(\mathbf{Q}) \exp(2i\mathbf{Q}\cdot\boldsymbol{e}) + \Psi_T^*(\mathbf{Q}) \exp(3i\mathbf{Q}\cdot\boldsymbol{e}) \quad (4.2)$$

Substituting (4.1) and (4.2) into (3.1) gives us the long range part of the free energy.

Thus, the basic task to evaluate the free energy of the double diamond structure is to determine the form of the tetrapod. However its precise form has not been determined experimentally. Although a minimal surface model[13] has been applied to analyze the observed structure, it is unclear whether or not the form of a tetrapod actually follows the minimal surface condition. In the present treatment, we shall utilize an approximate form of the form factor.

First, we calculate the surface area and the volume of a tetrapod. We consider jointed four cylindrical struts, as shown, e.g., in Figure 5b. The radius of each cylinder is denoted by R. The angle Θ between two cylinders satisfies the relations

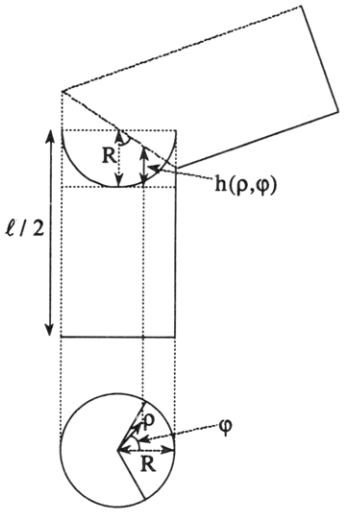

Figure 6. Cross section of a pair of cylinders in a tetrapod. The figure in the bottom shows a cross section of the cylinder.

$$\sin\frac{\Theta}{2} = \sqrt{\frac{2}{3}} \qquad \cos\frac{\Theta}{2} = \frac{1}{\sqrt{3}} \quad (4.3)$$

and is given by $\Theta = 109.47°$. As shown in Figure 6, it is convenient to divide a tetrapod into the joint and arm parts. The length of a cylinder in the arm part is $l/2 - R(1 - \cot(\Theta/2))$. We introduce the function $h(\rho,\phi)$ which stands for a "height" of the joint part. By a simple geometrical consideration, we obtain

$$h(\rho,\phi) = R - \frac{\rho}{\sqrt{2}}\cos\phi \quad (4.4)$$

Thus the volume J_V of the joint part is given by

$$J_V = 6\int_0^R d\rho \int_0^{\pi/3} d\phi\, \rho h(\rho,\phi) = R^3\left(\pi - \sqrt{\frac{3}{2}}\right) \quad (4.5a)$$

Similarly, we obtain the surface area J_A of the joint part as

$$J_A = 6R\int_0^{\pi/3} d\phi\, h(R,\phi) = 6R^2\left(\frac{\pi}{3} - \frac{\sqrt{6}}{4}\right) \quad (4.5b)$$

Adding the surface area and the volume of the arm parts to the above results, the total area S_T and the volume V_T of a tetrapod are given, respectively, by

$$S_T = 4l^2\left(\pi r - \frac{3\sqrt{6}}{2}r^2\right) \quad (4.6a)$$

$$V_T = 2l^3(\pi r^2 - \sqrt{6}r^3) \quad (4.6b)$$

where $r = R/l > 1/2$. The volume fraction f is related to V_T as $f = V_T/v_T$. In this way, the short range part of the free energy is given by

$$F_S = \frac{1}{2\rho_0 nN}\left(\frac{2N\sigma_A\hat{\gamma}}{l}\right) \quad (4.7a)$$

where

$$\hat{\gamma} = \frac{3\sqrt{3}}{2}\left(\pi r - \frac{3\sqrt{6}}{2}r^2\right) \quad (4.7b)$$

Next we calculate the long range part of the free energy. If one could calculate the form factor of the jointed

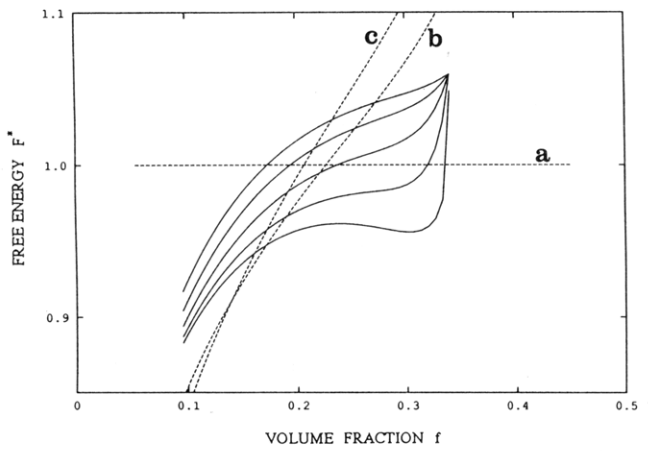

Figure 7. Equilibrium free energy of the diamond structure for R/p = 0.6, 0.7, 0.8, 0.9, and 1.0 from top to bottom. For comparison, the free energies of the lamellar (a), tetragonal (b) and bcc structures (c) are also displayed by the broken lines.

cylindrical struts, one would have obtained the total free energy without any ambiguity (apart from the question whether or not the tetrapod structure is well approximated by such struts). However, since the form factor of the jointed struts is quite complicated to evaluate, we here simplify the joint part by a sphere with radius p. Thus the length of a cylinder becomes $l/2 - p$. The lattice constant l is determined by the minimization of the free energy as for other structures discussed in the previous section. The radius R of the cylinder is determined for a given value of p by the condition that the volume fraction of the A domain in a unit cell is equal to f: $f = V_T/v_T$. The ratio R/p is regarded as an adjustable parameter. The form factor of a tetrapod can be written as

$$\Psi_T(\mathbf{Q}) = \Psi_S(\mathbf{Q}) + \sum_j \Psi_L(\mathbf{Q}_j) \tag{4.8a}$$

where

$$\Psi_S(\mathbf{Q}) = \frac{1}{2v_T}\frac{4\pi}{Q^3}\{\sin(pQ) - pQ\cos(pQ)\} \tag{4.8b}$$

and the summation in the second term in (4.8a) is taken for four cylinders. For a tetrapod shown in Figure 5b, the form factor of the cylinders is given by

$$\Psi_L(\mathbf{Q}_j) = \frac{1}{2v_T}\frac{2\pi R}{Q_{j\perp}}J_1(Q_{j\perp}R)\frac{2}{Q_{j\parallel}}\sin\left\{\frac{Q_{j\parallel}}{2}\left(\frac{l}{2} - p\right)\right\} \exp\left\{i\frac{Q_{j\parallel}}{2}\left(\frac{l}{2} + p\right)\right\} \tag{4.8c}$$

where $Q_{j\parallel}$ is the component of $\mathbf{Q}_j$ along the jth cylindrical axis while $\mathbf{Q}_{j\perp}$ is a two-dimensional vector perpendicular to $\mathbf{Q}_j$. The derivation of (4.8c) together with the definition of $\mathbf{Q}_j$ is given in Appendix B.

Substituting (4.8) into (4.1) and (4.2), we can calculate the long range part F_L

$$F_L = \frac{1}{2\rho_0 nN}\left(\frac{l^2\Phi}{N}\right) \tag{4.9}$$

where

$$\Phi = \sum_{\hat{\mathbf{Q}}}\frac{1}{\hat{Q}^2}\{2A_L^{AA} + 2A_L^{AC}\exp(2i\mathbf{Q}\cdot\mathbf{e})\}\Psi_A(\hat{\mathbf{Q}})\Psi_A^*(\hat{\mathbf{Q}}) \tag{4.10}$$

with $\hat{\mathbf{Q}} = \mathbf{Q}p$.

We have evaluated (4.10) numerically. The equilibrium free energy obtained is shown in Figure 7. By changing the ratio R/p, the free energy changes rather substantially.

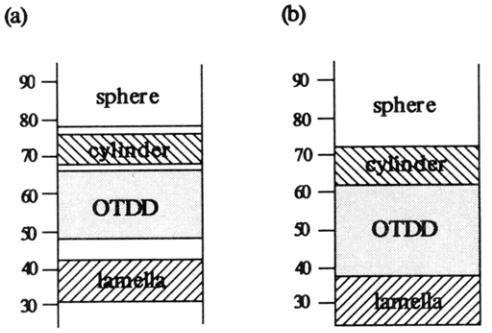

Figure 8. (a) Experimental phase diagram. The vertical axis indicates the volume fraction of the middle segment, i.e., $1 - 2f$. OTDD means ordered tricontinuous double diamond structure. (b) Theoretical phase diagram. The parameter R/p has been chosen as $R/p = 0.9$.

All the lines meet at $f = \sqrt{3}\pi/16 \approx 0.34$. This is the point where the arm length $l/2 - p$ becomes zero. Beyond this point, i.e., $f > 0.34$, the tetrapod picture breaks down in the present approximation. When R is close to zero, the free energy is larger than other structures such as lamellar and cylindrical ones. This means that a tetrapod with a small arm radius is unfavorable. On the other hand, when $p \approx R$, the free energy becomes smaller than those of lamellar and cylindrical domains. This clearly indicates that the diamond structure can appear in some range of the volume fraction. Although the present analysis with the adjustable parameter R/p does not predict the precise value of the critical volume fraction, the results obtained imply that formation of a diamond structure is quite possible near the transition region between the lamellar and the cylindrical structures.

In Figure 8, we summarize the phase diagram in the strong segregation for symmetric block copolymers. Figure 8a shows the experimental results obtained by Matsushita et al.[10] This should be compared with our theoretical results in Figure 8b where we have set $R/p = 0.9$ for the diamond structure. One can see that the theory is in fair agreement with the experiment.

5. Discussion

In this paper, we have investigated microphase separation of symmetric ABC-type triblock copolymers. As in a diblock copolymer, the long range interaction between the concentration fluctuations appears in the free energy functional. It originates from the chain connectivity and is one of the most important properties in the strong segregation limit. Keeping the long range interaction only up to the lowest order in the density expansion, we calculated the equilibrium free energy of various ordered structures.

We do not claim that the present result for the diamond structure is quantitatively correct. The long range part of the free energy was calculated by employing the crude approximation for the tetrapod form factor which contains one adjustable parameter. We have examined our approximation applying to diblock copolymers. That is, we calculated the equilibrium free energy of the double diamond structure starting with the free energy functional given in ref 4. The results are shown in Figure 9 where the free energies of the lamellar, cylindrical, and spherical structures are also displayed. If $R/p < 0.8$, the free energy of the double diamond structure is higher than any other structures. Anderson and Thomas obtained a similar result[13] where they utilized a model of constant-mean-curvature surfaces for tetrapods. One difficulty in our theory is, however, that the free energy of the diamond

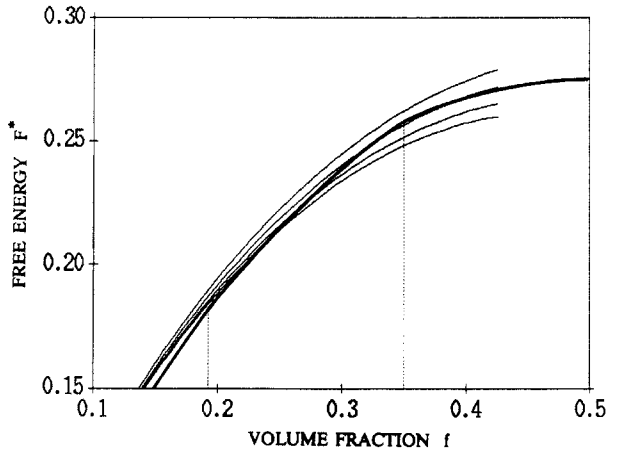

Figure 9. Equilibrium free energy for a diblock copolymer. The thick line indicates the free energy for lamellar, cylindrical (hexagonal), and spherical (bcc) structures. The critical block ratios for these structures are shown by the vertical dotted lines. The free energy for the double diamond structure is shown by thin lines for R/p = 0.7, 0.8, 0.9, and 1.0 from top to bottom.

structure becomes smaller than that of the lamellar one for $R/p > 0.9$ so that the lamellar phase disappears. (For $R/p = 0.8$, the diamond structure can exist in the narrow interval between the lamellar and the cylindrical phases.) In the triblock case, there appears the special volume fraction $f = 0.34$, which is the upper bound for the existence of the diamond structure. We do not have such a point in the diblock copolymers for the block ratio $f < 1/2$.

In these circumstances, what one needs is more information about the shape of the tetrapod. If it is available, it enables us to understand the tricontinuous ordered structures more definitely. It would also be interesting to apply the constant-mean-curvature surface model to ABC triblock copolymers. However, we did not carry out this in this paper because the form factor of a tetrapod calculated from the minimal surface model was not given explicitly in ref 13.

Despite the uncertainty for the diamond structure, we have the following results which are new for triblock copolymers: (1) The period of the ordered structure obeys the two-thirds power law, as in the case of diblock copolymers.[2,4] (2) In the cylindrical morphology, a square lattice is most stable. (3) In the spherical domains, a body centered cubic structure has the lowest free energy among others studied. The result (1) is consistent with that of Spontak and Zielinski.[16] It is emphasized here that the results (2) and (3) which were predicted independently with the experiments are entirely consistent with those obtained by Matsushita et al.[9] The critical volume fractions of the morphological transitions also exhibit satisfactory agreement with the experiments.

Acknowledgment. We are grateful for Professor Ichiro Noda and Dr. Yushu Matsushita for a number of valuable discussions. We are indebted to Mr. N. Suematsu who kindly calculated the volume of a tetrapod.

Appendix A

Here we summarize the formulas associated with the matrix M in (2.15). The components of the inverse matrix Γ defined by (2.11) can readily be obtained since those are the density correlations of a single Gaussian chain. After Fourier transform, the components are given by

$$\Gamma_q^{AA} = n^2 h_q(Nf_A) \qquad \Gamma_q^{BB} = n^2 h_q(N(1-f_A-f_C)) \qquad \Gamma_q^{CC} = n^2 h_q(Nf_C)$$

$$\Gamma_q^{AB} = \Gamma_q^{BA} = n^2 g_q(Nf_A, 0, N(1-f_A-f_C))$$

$$\Gamma_q^{AC} = \Gamma_q^{CA} = n^2 g_q(Nf_A, N(1-f_A-f_C), f_C) \quad \text{(A.1)}$$

$$\Gamma_q^{BC} = \Gamma_q^{CB} = n^2 g_q(N(1-f_A-f_C), 0, Nf_C)$$

where

$$h_q(x) = 2x^2\left[\frac{2}{q^2x} - \left(\frac{2}{q^2x}\right)^2\left\{1 - \exp\left(-\frac{q^2x}{2}\right)\right\}\right] \quad \text{(A.2)}$$

$$g_q(x,y,z) = -\frac{4}{q^2}\left[\exp\left\{-\frac{q^2(x+y)}{2}\right\} + \exp\left\{-\frac{q^2(y+z)}{2}\right\} - \exp\left\{-\frac{q^2(x+y+z)}{2}\right\} - \exp\left\{-\frac{q^2y}{2}\right\}\right] \quad \text{(A.3)}$$

These two functions have the following asymptotic limits:

(i) $q^2 \ll 1$

$$h_q(x) = x^2\left(1 - \frac{q^2x}{6}\right)$$

$$g_q(x,y,z) = xz\left\{1 - \frac{q^2(x+2y+z)}{4}\right\} \quad \text{(A.4)}$$

(ii) $q^2 \gg 1$

$$h_q(x) = \frac{4x}{q^2} \qquad g_q(x,y,z) = \begin{cases} \frac{4}{q^2} & \text{for } y = 0 \\ 0 & \text{for } y \neq 0 \end{cases} \quad \text{(A.5)}$$

By using these results, the elements of the 3 × 3 matrix are calculated for $q \to \infty$ and for $q \to 0$, respectively as

$$\mathrm{M}_q = \frac{q^2}{n^2N}\frac{1}{4f_Af_C(1-f_A-f_C)} \times \begin{pmatrix} f_C(1-f_A-f_C) & 0 & \\ & f_Af_C & \\ 0 & & f_A(1-f_A-f_C) \end{pmatrix} \quad \text{(A.6)}$$

$$\mathrm{M}_q = \frac{1}{q^2n^2N^3}A' \times \begin{pmatrix} \frac{2(1-f_A)}{f_A^2} & \frac{3f_A+f_C-3}{f_A(1-f_A-f_C)} & \frac{1-f_A-f_C}{f_Af_C} \\ \frac{3f_A+f_C-3}{f_A(1-f_A-f_C)} & \frac{2(3-2f_A-2f_C)}{(1-f_A-f_C)^2} & \frac{f_A+3f_C-3}{f_C(1-f_A-f_C)} \\ \frac{1-f_A-f_C}{f_Af_C} & \frac{f_A+3f_C-3}{f_C(1-f_A-f_C)} & \frac{2(1-f_C)}{f_C^2} \end{pmatrix} \quad \text{(A.7)}$$

where

$$A' = \frac{6}{3 - 2(f_A+f_C) - (f_A-f_C)^2} \quad \text{(A.8)}$$

From (A.6) and (A.7) we obtain (2.18) with (2.20)–(2.24) after elimination of ρ_B.

Appendix B

In this Appendix, we derive the form factor of the arm parts of a tetrapod. As shown in Figure 10, we need a

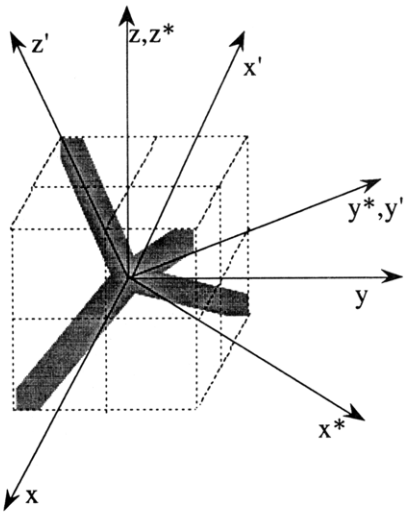

Figure 10. Rotation of the coordinates from (x, y, z) to (x', y', z').

coordinate transformation from (x, y, z) to (x', y', z') where the z' axis is along the cylindrical axis of one of the arms. This can be achieved by two successive rotations:

$$\mathbf{r} = \mathbf{R}_2\mathbf{R}_1\mathbf{r}' \tag{B.1}$$

where

$$\mathbf{R}_1 = \begin{pmatrix} \cos\frac{\Theta}{2} & 0 & -\sin\frac{\Theta}{2} \\ 0 & 1 & 0 \\ \sin\frac{\Theta}{2} & 0 & \cos\frac{\Theta}{2} \end{pmatrix}$$

$$\mathbf{R}_2 = \begin{pmatrix} \cos\frac{\pi}{4} & -\sin\frac{\pi}{4} & 0 \\ \sin\frac{\pi}{4} & \cos\frac{\pi}{4} & 0 \\ 0 & 0 & 1 \end{pmatrix} \tag{B.2}$$

The angle Θ is the angle between the two arms. The reciprocal lattice vector $\mathbf{Q}$ is, then, transformed as

$$\mathbf{Q}_1 = \mathbf{Q}\mathbf{R}_2\mathbf{R}_1 \tag{B.3}$$

Thus the form factor of the first cylinder is given by (4.8c) with $\mathbf{Q}_j = \mathbf{Q}_1$.

As can be readily seen from Figure 10, the form factor of the remaining cylinders can be obtained from (4.8c) by rotation of $\mathbf{Q}_1$. That is, we introduce two matrices:

$$\mathbf{R}_3 = \begin{pmatrix} \cos\Theta & 0 & \sin\Theta \\ 0 & 1 & 0 \\ -\sin\Theta & 0 & \cos\Theta \end{pmatrix}$$

$$\mathbf{R}_4(\varphi) = \begin{pmatrix} \cos\varphi & -\sin\varphi & 0 \\ \sin\varphi & \cos\varphi & 0 \\ 0 & 0 & 1 \end{pmatrix} \tag{B.4}$$

The form factors $\Psi_L(\mathbf{Q}_j)$ $(j = 2\text{–}4)$ are the same form as those of (4.8c) but with the arguments

$$\mathbf{Q}_j = \mathbf{Q}_1\mathbf{R}_4\left(\frac{2\pi}{3}(j-2)\right)\mathbf{R}_3 \tag{B.5}$$

References and Notes

(1) Helfand, E.; Wasserman, Z. R. *Macromolecules* **1980**, *13*, 994 and the earlier references cited therein.
(2) Semenov, A. N. *Zh. Eksp. Teor. Fiz.* **1985**, *88*, 1242; *Sov. Phys. JETP* **1985**, *61*, 733.
(3) Leibler, L. *Macromolecules* **1980**, *13*, 1602.
(4) Ohta, T.; Kawasaki, K. *Macromolecules* **1986**, *19*, 2621.
(5) Ohta, T.; Kawasaki, K. *Macromolecules* **1990**, *23*, 2413.
(6) Melenkevitz, J.; Muthukumar, M. *Macromolecules* **1991**, *24*, 4199.
(7) Shull, K. R. *Macromolecules* **1992**, *25*, 2122.
(8) Kawasaki, K.; Kawakatu, T. *Macromolecules* **1990**, *23*, 4006.
(9) Mogi, Y.; Kotsuzi, H.; Kaneko, Y.; Mori, K.; Matsushita, Y.; Noda, I. *Macromolecules* **1992**, *25*, 5408.
(10) Mogi, Y.; Mori, K.; Matsushita, Y.; Noda, I. *Macromolecules* **1992**, *25*, 5412; unpublished work.
(11) Hashimoto, T.; Tanaka, H.; Hasegawa, H. In *Molecular Conformation and Dynamics of Macromolecules in Condensed Systems*; Nagasawa, M., Ed.; Elsevier, Amsterdam, 1988.
(12) Thomas, E. L.; Alward, D. B.; Kinning, D. J.; Handlin, D. L.; Fetters, L. J. *Macromolecules* **1986**, *19*, 2197.
(13) Anderson, D. M.; Thomas, E. L. *Macromolecules* **1988**, *21*, 3221.
(14) Hasegawa, H.; Tanaka, H.; Yamasaki, K.; Hashimoto, T. *Macromolecules* **1987**, *20*, 1651.
(15) Spontak, R. J.; Smith, S. D.; Ashraf, A. *Macromolecules* **1993**, *26*, 956. Winey, K. I.; Thomas, E. L.; Fetters, L. J. *Macromolecules* **1992**, *25*, 422.
(16) Spontak, R. J.; Zielinski, J. M. *Macromolecules* **1992**, *25*, 663.
(17) Kawasaki, K.; Ohta, T.; Kohrougi, M. *Macromolecules* **1988**, *21*, 2972.
(18) Atkins, P. W. *Physical Chemistry*; Oxford University Press: London, 1982.
(19) Kittel, C. *Introduction to Solid State Physics*; John Wiley & Sons: New York, 1986.